One-pot fabrication of hydrophobic, superelastic, harakeke-derived nanocellulose aerogels with excellent shape recovery for oil adsorption and water-in-oil emulsion separation

Yitong Zhai, Xiaowen Yuan

PII: S0141-8130(24)06297-4

DOI: https://doi.org/10.1016/j.ijbiomac.2024.135489

Reference: BIOMAC 135489

To appear in: *International Journal of Biological Macromolecules*

Received date: 27 May 2024

Revised date: 28 August 2024

Accepted date: 7 September 2024

Please cite this article as: Y. Zhai and X. Yuan, One-pot fabrication of hydrophobic, superelastic, harakeke-derived nanocellulose aerogels with excellent shape recovery for oil adsorption and water-in-oil emulsion separation, *International Journal of Biological Macromolecules* (2024), https://doi.org/10.1016/j.ijbiomac.2024.135489

One-pot fabrication of hydrophobic, superelastic, harakeke-derived nanocellulose aerogels with excellent shape recovery for oil adsorption and water-in-oil emulsion separation

Yitong Zhai[a], Xiaowen Yuan[a*]

[a] Future Fibres Laboratory, School of Engineering, Computer and Mathematical Sciences, Auckland University of Technology, Auckland, New Zealand.

[*]Corresponding author: Xiaowen Yuan

E-mail: xiaowen.yuan@aut.ac.nz

Phone: +64 9 921 9999 ext 7320

Abstract

Cellulose-based aerogels have attracted significant attention for oil/water separation due to their high porosity, large specific surface area and high adsorption capacity. However, their intrinsic hydrophilicity, and inadequate mechanical properties have often limited their practical applications. Traditional freeze-dried cellulose aerogels exhibit unsatisfactory elasticity and require a separate surface modification process to adjust the surface wettability. In this study, we present a novel one-pot fabrication strategy which simultaneously achieves the crosslinking of individual cellulose nanofibers and the hydrophobic modification of the surface wettability. Following directional freeze-drying, hydrophobic, superelastic, and anisotropic cellulose-based aerogel was prepared from the 2,2,6,6-tetramethylpiperidin-1-oxyl (TEMPO)-oxidized cellulose nanofibers, isolated from harakeke (New Zealand native flax). The resulting aerogel exhibits a high water contact angle of 142°, good compressive recovery performance (85% recovery of the original height after 100 compression cycles at 70% strain), and outstanding adsorption capacity for various types of oil and organic solvents (80 – 105 g/g). Furthermore, the aerogel could also be used as a filter to separate the surfactant stabilized water-in-oil emulsions with high flux (782 L m^{-2} h^{-1}) and high separation efficiency (98.7-99.2%). The novel aerogel prepared in this study is expected to have great potential for practical applications in oily wastewater remediation.

Keywords

Harakeke, Cellulose aerogel, Oil adsorption, Filtration, Superelastic

1. Introduction

Oil spills occurring during oil extraction and marine oil transportation represent a significant environmental catastrophe which can lead to substantial economic losses and pose serious threats to marine ecosystems and human health [1]. Among the various methods for oil spill remediation, physical adsorption is considered the most promising due to its simplicity, environmental friendliness, and sustainability. Traditional oil sorbents are typically classified into three categories, 1) plant fibers, such as kapok fiber [2], sugarcane bagasse [3], and rice husks [4], which have good biodegradability, but poor in adsorption capacity; 2) inorganic minerals, such as, clay and zeolite are inexpensive but difficult to recycle and poor in buoyancy; 3) synthetic polymer-based sorbents, including polyurethane foams [5] and polypropene fiber [6], which exhibit good oil adsorption selectivity, but suffer from poor biodegradability and require complicated preparation processes.

In recent years, aerogels have attracted significant attention from researchers as potential oil sorbents due to their highly porous structure, large specific surface area, and low density. However, the first generation of silica aerogels are fragile and lack mechanical strength, while the second generation of synthetic polymer-based aerogels are non-biodegradable and may lead to the problem of secondary pollution. Cellulose-based aerogels, representing the third generation, not only inherit the advantages of traditional aerogels, but are also biodegradable and exhibit high oil adsorption capacities [7]. Nevertheless, the practical applications are impeded by their inherent hydrophilicity (poor oil/water selectivity), and inferior mechanical properties (poor shape recovery under small deformation). Various strategies have been employed to enhance the hydrophobicity and mechanical properties of cellulose-based aerogels, including chemical vapor deposition (CVD), atomic layer deposition (ALD), carbonization under inert gas atmosphere, and surface-initiated atom transfer radical polymerization (SI-ATRP) [8]. Among these, CVD is the most widely utilized method; however, it suffers from drawbacks such as non-uniform modification within the aerogel and strict reaction conditions [9]. Thus, there is an urgent need for a more facile approach to uniformly modify the surface wettability of cellulose-based aerogels. To improve the mechanical robustness of cellulose aerogels, the incorporation of flexible yet durable solid constituents has become the primary strategy [10]. Graphene and carbon nanotubes (CNTs) are commonly used due to their inherent robustness and macroscopic flexibility. For example, Zhou et al. [11] prepared a graphene/polyvinyl alcohol/cellulose nanofiber aerogel by simply mixing together the water solution of individual components in a mass ratio of 1:1:1.5, followed by freeze-drying to obtain the aerogel. The aerogel was then carbonized in a tube furnace at 500 °C for 120 min to yield a hydrophobic surface wettability. Although the resulting aerogel showed good hydrophobicity with high oil adsorption capacity and achieved good recyclability through an adsorption-combustion method, the preparation process is time-consuming and complicated, and the graphene precursor is expensive. Moreover, to recover the absorbed oil from the aerogel body, mechanical squeezing is widely applied due to its simplicity and cost-effectiveness [12]. However, most reported cellulose-based aerogels suffer from poor mechanical robustness, exhibiting low shape recovery rate after compression, which leads to a significant decline in the oil adsorption capacity after mechanical squeezing. Therefore, developing cellulose-based aerogels with high hydrophobicity, good compression robustness, and cost-effective precursors through a simple process is of great importance.

Previous research has identified the nonelastic microstructure of cellulose-based aerogels as a key factor contributing to their lack of elasticity [13]. Directional freeze-casting has been proposed as a method to regulate the microstructure, thereby enhancing their mechanical robustness. This process involves the directional freezing of a suspension followed by lyophilization. The resultant aerogels exhibit a highly ordered lamellar structure, which significantly improves their mechanical properties [14]. Additionally, the formation of strong chemical bonds to link individual cellulose nanofibers

(CNFs) is believed to further enhance their mechanical performance. Therefore, in this study, we report a facile one-pot fabrication strategy to prepare crosslinked, hydrophobic, and highly compressible cellulose-based aerogels from harakeke (a variety of New Zealand native flax). After extracting the CNFs from harakeke, 1,2-Bis(trimethoxysilyl)ethane (BTMSE) and methyltriethoxysilane (MTES) were added into the CNFs suspension, serving as a crosslinking agent and hydrophobic modifier, respectively. This approach achieves both the chemical crosslinking of CNFs for mechanical strengthening and the hydrophobic modification of the cellulose aerogel in a single step, thereby greatly simplifying the aerogel preparation process. To the best of our knowledge, this is the first time in which the mechanical properties and hydrophobicity of cellulose-based aerogels have been simultaneously optimized. Previous studies involving acid hydrolysis silane modification (AHSM) of cellulose-based aerogels mainly focused on using methyltrimethoxysilane (MTMS). Our study also addresses the need for the exploration of more types of silanes for the modification of cellulose-based aerogels via the AHSM method [15].

2. Experimental section

2.1 Materials

Harakeke fiber was provided by a local Auckland company. 2,2,6,6-tetramethylpiperidin-1-oxyl (TEMPO), sodium bromide, sodium hypochlorite solution (available chlorine 10-15%), acetic acid, potassium hydroxide, toluene, ethanol, 1,2-Bis(trimethoxysilyl)ethane (BTMSE), and methyltriethoxysilane (MTES) were purchased from Sigma Aldrich (Saint Louise, USA).

2.2 Preparation of TEMPO oxidized CNFs from raw harakeke

The TEMPO oxidized CNFs were extracted from raw harakeke fibers based on our previous work with minor modifications [16]. The raw harakeke fibers were first shredded and sieved through a 60 mesh screen, then the wax and oily contaminants were removed using the Soxhlet extraction method with a mixture of toluene/ethanol (volume ration, 2:1) at 90 °C for 8 h and the powder dried in an oven. Next, the harakeke powder was delignified using 2 wt% acidic (acetic acid, pH = 4) sodium hypochlorite solution at 70 °C for 2 h. This delignification treatment was repeated four times. Subsequently, the fiber was treated with 2 wt% potassium hydroxide at 90 °C for 2 h to remove the hemicellulose. The chemically purified fibers (10 g) were then stirred in distilled water (1 L) with TEMPO (0.2 g) and sodium bromide (1.2 g). The desired amount of sodium hypochlorite solution was added dropwise into the CNF suspension while stirring. Then the pH of the suspension was adjusted to 10 using 0.1 M sodium hydroxide solution. Finally, the TEMPO oxidized fibers were washed with distilled water to neutral pH and stored at 4 °C. The CNFs were prepared by ultrasonication of the TEMPO-oxidized fibers (0.5 wt%) using a probe ultrasonicator (UP400St, Hielscher, Germany) at 50% power in an ice/water bath for 30 mins.

2.3 One-pot fabrication of hydrophobic and anisotropic cellulose aerogel by directional freeze-casting

To facilitate the hydrolysis of BTMSE and MTES, and their further reaction with CNFs, the pH of the CNF suspensions (50 g) was adjusted to 4 using acetic acid. Then 0.25 g BTMSE was added into the CNF suspension dropwise under vigorous stirring. After stirring at room temperature for 2 h, different amounts of MTES (Table S1) were added dropwise into the CNF suspension, while the suspension was kept stirring for another 2 h. Subsequently, the CNF suspension was pre-cooled to 4 °C.

Anisotropic cellulose-based aerogels were prepared using a direct freeze-drying technique with a custom-made mold (Fig. S1), consisting of a rectangular polytetrafluoroethylene (PTFE) surround attached to a brass plate at the bottom. Typically, the prepared cellulose nanofiber (CNF) suspension was poured into the mold, followed by freezing only the bottom brass plate by immersing it in liquid nitrogen (-196 °C) for 30 minutes. During freezing, the PTFE surround acted as a thermal barrier, isolating the cold, while the brass plate, immersed in liquid nitrogen, transferred the cold from the bottom to the CNF suspension. This created a temperature gradient along the vertical direction, driving the ice crystals to grow vertically from the bottom to the top. The frozen sample was then stored in the cold trap of the freeze-dryer (DGJ-10E, Shanghai Boden Biological Technology Co., Ltd., China) at -60 °C for 2 hours to stabilize the structure. Subsequently, the samples were freeze-dried at -60 °C under vacuum for another 48 hours. For comparison, isotropic cellulose aerogels made from conventional freeze-drying were also prepared by directly immersing the silylated CNF suspension into liquid nitrogen.

2.4 Density and porosity of the aerogel

The apparent densities were calculated by measuring the mass and volume of the aerogels.

$$\rho = \frac{m}{v} \tag{1}$$

where ρ is the density (g/cm^3), and m and v are the mass (g) and volume (cm^3) of the of the aerogel respectively.

The porosity is calculated using the following equation

$$P = \left(1 - \frac{\rho}{\rho_s}\right) \times 100\% \tag{2}$$

where P is the porosity (%) of the aerogel, and ρ_s is the density (g/cm^3) of the aerogel skeleton.

Because the hydrophobic cellulose-based aerogel is a composite aerogel of CNFs and polysiloxane, the density of the solid scaffold was calculated according to equation (3).

$$\rho_s = \frac{1}{\frac{W_{CNF}}{\rho_{CNF}} + \frac{W_{polysiloxane}}{\rho_{polysiloxane}}} \tag{3}$$

where W and ρ are the weight fraction and density of the corresponding materials respectively. The density of CNF is taken as 1.5 g/cm^3 [17], and the density of polysiloxane is taken as 1.9 g/cm^3 based on the literature [18].

2.5 Characterization

The morphology of the prepared cellulose nanofibers was observed using an atomic force microscope (Cypher-ES AFM, Asylum Research Ltd.). A dilute drop of aqueous CNF suspension (0.05 wt%) was dispersed on the surface of mica and air-dried 12 h. The fibers were examined by dynamic force mode (tapping mode), using a Tap300Al-G probe (Budget Sensors) with a spring constant of 42 N/m, at the resonance frequency of 300 kHz. The crystal information of the fibers was characterized by X-ray diffraction (XRD, Bruker D8 Advance, Germany) with Cu-K α radiation (λ= 1.5418 Å) at a scan rate of 4°/min, 40 kV, 40 mA ranging from 5° to 50°. A scanning electron microscope (SEM, Hitachi S-4800, Japan) was used to observe the morphology of the prepared aerogels at acceleration voltage of 5 kV. The aerogel was immersed in liquid nitrogen and then cut both parallel and perpendicular to the ice crystal growth direction using a razor blade. The chemical structure of the aerogels was studied using Fourier transform infrared (FT-IR, Nicolet IS10 FT-IR spectrometer, Thermo Fisher Scientific, USA) scanning between 600–4000 cm^{-1} with a resolution of 6 cm^{-1}. The surface composition of the aerogels was investigated using X-ray photoelectron spectroscopy (XPS, Thermo Fisher Escalab 250Xi, US). The thermal stability of the aerogel was studied using a thermogravimetric analyser (TGA, TA Instruments, USA) from room temperature to 800 °C at a heating rate of 10 °C/min under N_2 protection. The surface wettability of the aerogel was investigated by measuring the static water contact angle using a contact angle goniometer (OCA20, Dataphysics Instrument, Germany). 5 μL of water was applied to the surface of the aerogel and the contact angles were recorded. Each sample was measured 5 times at different positions, and the average value was recorded.

2.6 Compression test

The compression test was performed using an Instron 5848 testing system (Instron Co. UK) equipped with a 50 N load cell. Cubic samples with dimensions of 20 mm × 20 mm × 30 mm were compressed in both the longitudinal and transverse directions to 80% of its original height with a strain rate of 5 mm/min to record the stress-strain curve. Compression modulus was determined from the initial linear region of the stress-strain curve. For the cyclic compression-release test, the strain was applied in the transverse direction, the strain rate was set to 100 mm/min and 100 cycles were applied. Three repetitions were performed on each sample.

The shape recovery rate (S, %) was determined by the following equation:

$$S = \frac{h_{after}}{h_{before}} \times 100\% \tag{4}$$

where h_{before} and h_{after} are the height of sample before and after the test respectively.

2.7 Oil adsorption, water/oil emulsion separation performance and reusability of aerogel

Different types of oils and organic solvents were used to characterize the oil adsorption performance of the aerogels. The aerogel was weighed before the test and then immersed in the testing oil to reach adsorption equilibrium. Next the aerogel was taken out of the oil and placed on a steel mesh for 1 min to drain the surface of excessive oil. Then the aerogel was weighed again. The adsorption capacity (Q, g/g) of the aerogel was calculated by equation (5)

$$Q = \frac{m_a - m_0}{m_0} \tag{5}$$

Where m_o and m_a are the weights of aerogel before and after oil adsorption respectively.

The reusability of the aerogel was investigated by cyclic adsorption-squeezing test. After recording the weight, the oil adsorbed aerogel was squeezed using two parallel glass plates to about 20% of its original height to release the adsorbed oil. Then the aerogel was immersed back in the oil for the second oil adsorption test. This process was repeated 10 times for each sample, and the oil adsorption capacity was recorded after each cycle.

The water-in-oil emulsions were prepared according to a previous study [19]. Briefly, a certain amount of oil to be tested was mixed with 0.1 wt% span 80 and 2 wt% water. Then the mixture was stirred by an IKA T25 digital ULTRA TURRAX blender at a speed of 12000 rpm for 15 min to form a stable milky emulsion. The resultant surfactant stabilized emulsion was stable for more than one month without demulsification. The water droplet sizes were measured using an optical microscope. For emulsion separation, the as-prepared aerogel was place at the bottom of the filtering apparatus and then the emulsion was loaded into the chamber. The separation process is driven solely by gravity. The flux (F, L $m^{-2}h^{-1}$) of the aerogel filter was calculated according to equation (6)

$$F = \frac{V}{A \times t} \tag{6}$$

where, V is the total amount of oil that flowed through the aerogel, A is the cross-section area of the aerogel, and t is the separation time.

The water concentration in the emulsion and filtered oil were determined using a Karl Fischer titrator, and the separation efficiency was determined by equation (7).

$$E = \frac{C_0 - C_1}{C_0} \times 100\% \tag{7}$$

where, C_0 is the water concentration in the as-prepared emulsion, and C_1 is the water concentration in the filtered oil.

3. Results and discussion

3.1 Structural and chemical characterization

The CNFs used in this study were extracted from harakeke through a process involving chemical purification, TEMPO oxidization and ultrasonication as previously reported by our group [17]. As shown in Fig. S2, raw harakeke fiber, comprised of aligned tracheids with diameter of approximately 200 μm were successfully converted into CNFs with an average diameter of 8 – 30 nm. FTIR spectra (Fig. S3) confirms the successful removal of lignin and hemicellulose during the chemical purification process. Specifically, the band at 1507 cm^{-1} is ascribed to the aromatic C-O skeleton vibration of lignin, the band at 1733 cm^{-1} due to the C=O stretching, and the band at 1239 cm^{-1} due to the C-O-C vibration of hemicellulose in the raw harakeke, all disappeared in the chemically purified fibers [20]. The bands at 1591 cm^{-1} and 1412 cm^{-1}, primarily caused by the vibration of the C=O bond of carboxyl groups, indicate the hydroxyl groups at the C6 position for cellulose have been converted into sodium carboxylates by the TEMPO oxidization [21].

Fig. 1a shows a schematic illustration of the one-pot fabrication of hydrophobic, highly compressible and anisotropic cellulose aerogel. After the extraction of CNFs from raw harakeke, BTMSE and MTES were added dropwise into the CNF suspension to initiate the modification reaction. The anisotropic cellulose-based aerogel was obtained by pouring the modified CNF suspension into the mold for directional freezing followed by freeze-drying. The mechanism of this AHSM is depicted in Fig. 1b. In this process, BTMSE and MTES were added into the acidic CNF suspension as crosslinker and hydrophobic modifier, respectively. Under acidic conditions, BTMSE and MTES first underwent hydrolysis, leading to the formation of reactive silanols (Si-OH). Two reactions then occurred simultaneously in the CNF suspension: 1) the silanol groups reacted with the hydroxyl groups of CNFs through dehydration, forming Si-O-C bonds; 2) the silanol groups underwent self-condensation, forming stable Si-O-Si bonds, which resulted in the creation of polysiloxane particles. After freeze-drying, cellulose-based aerogels crosslinked by BTMSE with a hydrophobic polysiloxane particle coated surface were obtained [18, 22].

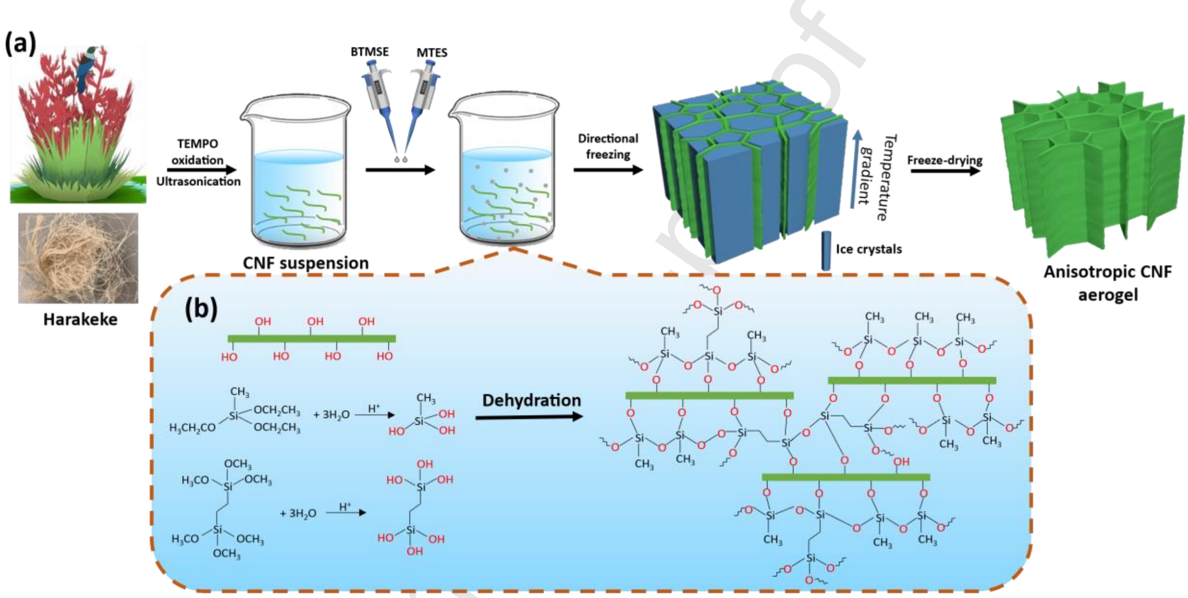

Fig. 1. (a) Schematic illustration of the preparation process of anisotropic cellulose aerogel; (b) mechanism of the AHSM process.

The crosslinking and hydrophobic modification were confirmed by FTIR and XPS analyses. As shown in Fig. 2a, compared to the pure CNF aerogels, the band intensity at 918 cm^{-1} in the BTMSE crosslinked aerogel increased due to the overlapping of new Si-OH, stretching the peak along with the anomeric C-H deformation peak [18]. Additionally, a new band appeared at 696 cm^{-1}, ascribed to the Si-O-C bond further confirming this chemical crosslinking mechanism [23]. For the MTES modified hydrophobic aerogels, two new bands at 2980 cm^{-1} and 775 cm^{-1} were assigned to the stretching vibration of C-H bonds of the $-CH_3$ terminal groups. The band at 1270 cm^{-1} was due to the vibration of the $Si-CH_3$ bond [24]. The new bands indicate the successful modification and formation of polysiloxane particles on the cellulose aerogel. Fig. 2b shows as the addition of MTES increases, the transmittance signal of 1270 cm^{-1} and 775 cm^{-1} increases, indicating the formation of more polysiloxane particles with increased MTES addition.

The interfacial bonding information was further studied using XPS analysis, as shown in Fig. 2c. The MTES modified aerogels exhibited four peaks corresponding to O, C, and Si elements in the full scan. In fig. 2d, the C spectrum shows three peaks at 283.8 eV, 285.5 eV and 286.9 eV, attributed to the C-C, C-O, and O-C-O bonds, respectively [17]. The spectrum of O 1s shows two peaks at 532.1 eV and 533.8 eV, corresponding to C–O and Si–O components, respectively (Fig. 2e). Additionally, the Si 2p spectrum was deconvoluted into the Si–O bond at 101.8 eV and the Si–C bond at 103.2 eV (Fig. 2f) [25]. Those results further demonstrated the successful salinization reaction and are in agreement with the FTIR data.

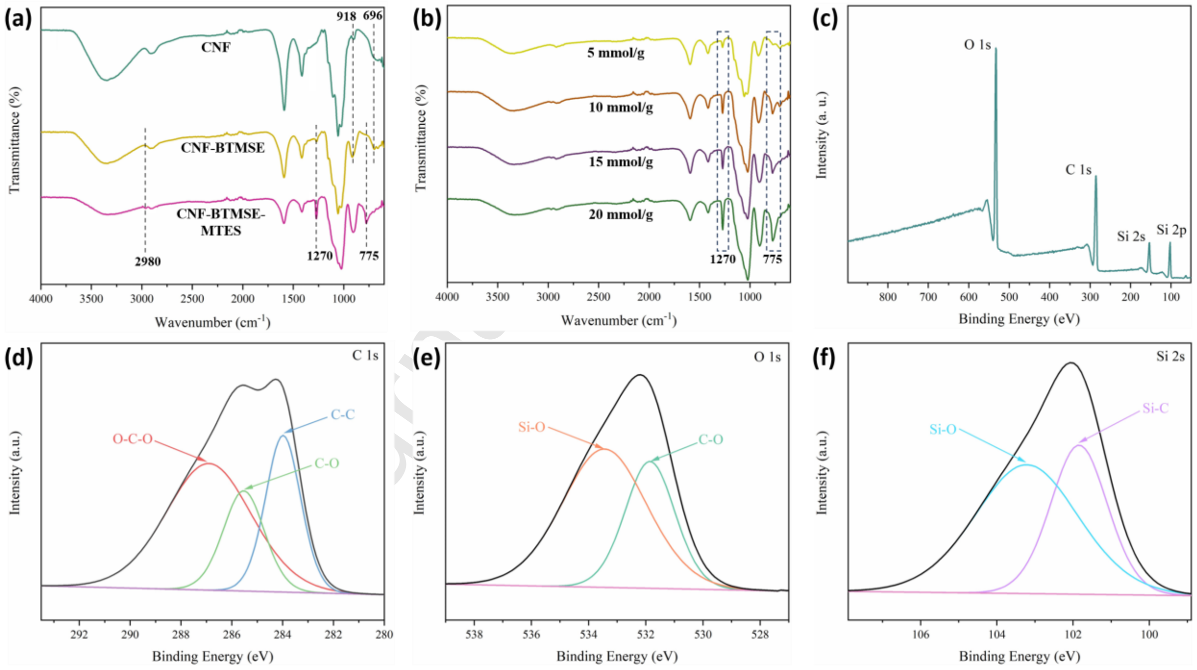

Fig. 2. (a) FTIR spectra of CNF, CNF-BTMSE, and CNF-BTMSE-MTES aerogels; (b) FTIR spectra of CNF-BTMSE-MTES aerogels with different MTES additions; (c) Full-survey scan XPS spectrum of 10 mmol/g MTES modified aerogels; (d-e) High-resolution XPS spectrum of C 1s, O 1s and Si 2p respectively.

Directional freezing is widely employed in the preparation of aerogels with anisotropic structures. The conventional freeze-drying method results in aerogels with isotropic structure due to the uncontrolled nucleation and growth of ice crystals. In contrast, directional freezing establishes a vertical temperature gradient between the bottom and top, promoting in the directional growth of ice crystals. During the directional freezing process, ice crystals initially formed homogenously at the bottom of the mold, and then grew vertically along the temperature gradient, extruding the CNFs alongside. Subsequently, the ice crystals sublimated during freeze-drying, leaving the aerogel with an anisotropic structure. Aerogels prepared by the conventional freeze-drying method with random porous structure show relatively lower oil adsorption efficiency because of the diffusion resistance caused by the disordered structure. In contrast, directionally freeze-dried aerogels exhibit an aligned channel structure which can generate capillary forces and shorten the oil transport path, enabling rapid oil adsorption against gravity [26]. As shown in Fig. S4, when a drop of Sudan-III stained vegetable oil was dropped on the aerogel, the red liquid was instantly diffused vertically from the top to the bottom of the aerogel with slow diffusion speed in the lateral direction. This diffusion path reflects the anisotropic microstructure of the aerogel.

SEM images were taken to study the structure and morphology differences of directional freeze-dried and conventional freeze-dried aerogels. As shown in Fig. 3a, the directional freeze-dried aerogel exhibits a 3-dimensioanl porous honeycomb-like structure consisting of corrugated channel with an oblate shape in cross-section (Fig. 3a_1- a_2). The longitudinal section of the aerogel showed a parallel tubular structure along the freezing direction (Fig. 3 a_3- a_4). Moreover, the high magnification image taken from the longitudinal section of the channel wall clearly shows the presence of polysiloxane particles, confirming the successful AHSM (Fig. a_5). In contrast, the conventional freeze-dried aerogel shows an isotropic structure composed of randomly distributed cellulose sheets (Fig. 3b_1-b_2). The density and porosity of the anisotropic aerogel are summarized in Table S1. With the increase in MTES concentration from 0 mmol/g_{CNF} to 25 mmol/g_{CNF}, the density of aerogels increased from 16.32 kg/m^3 to 21.89 kg/m^3, while the porosity decreased from 99.01% to 97.03%, this is attributed to the condensation of more polysiloxane particles on the CNF skeleton.

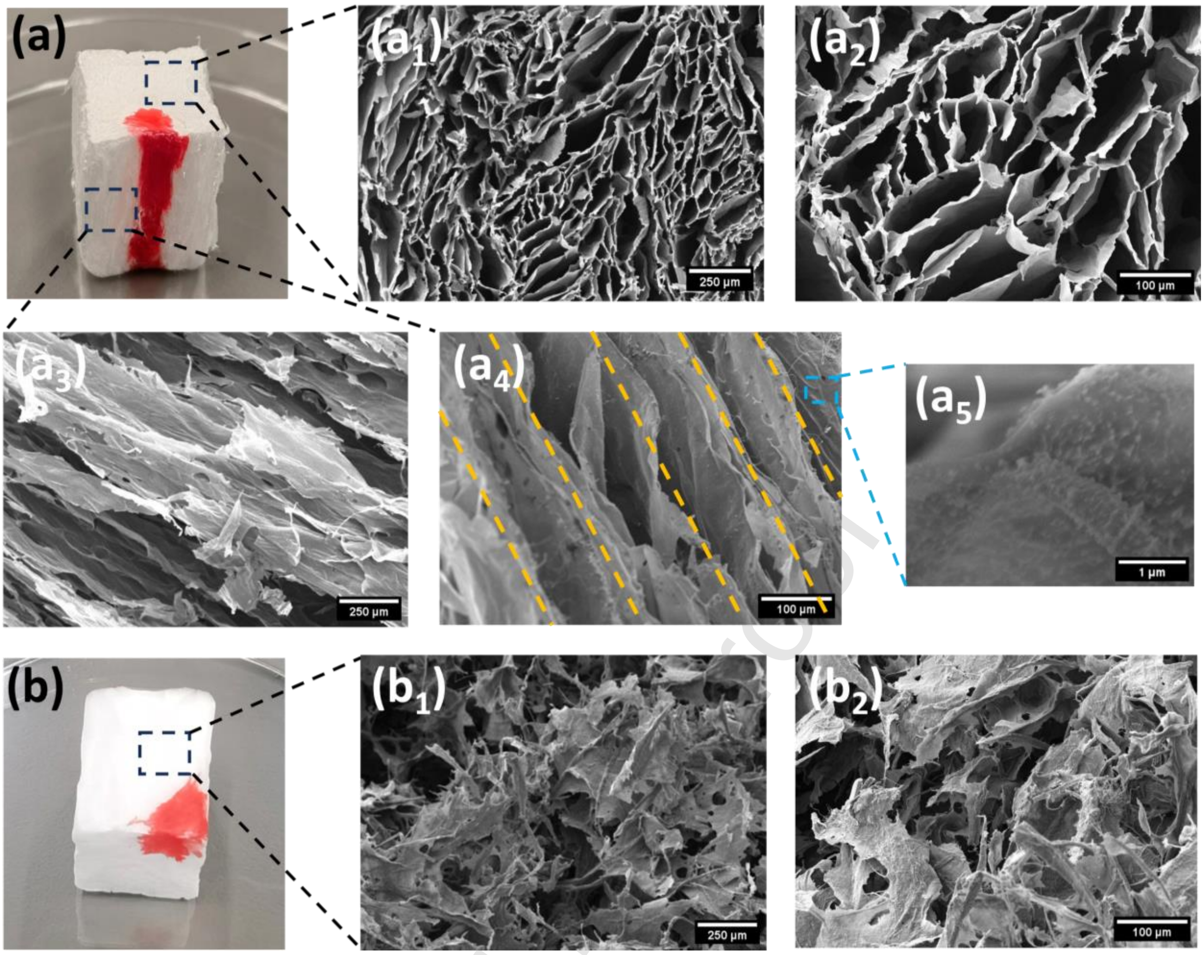

Fig. 3. (a) Directional freeze-dried aerogel, (a$_1$-a$_2$) SEM images showing the cross-section of anisotropic aerogel, (a$_3$-a$_5$) SEM images showing the side of the anisotropic aerogel; (b) Conventional freeze-dried aerogel, (b$_1$-b$_2$) SEM images showing the microstructure.

3.2 Mechanical properties

The compressive and resilience properties are critical for cellulose-based aerogels in determining their recyclability and durability for oil adsorption applications [27]. Given the anisotropic structure of the aerogel, compression tests were carried out in two directions; along the direction of the vertically aligned channels (denoted as “longitudinal direction”); and the direction perpendicular to the channels (denoted as “transverse direction”). The letter “l-” and “t-” represent the compression directions respectively (Fig. 4a). The compressive stress-strain curves of aerogels in both directions are shown in Fig. 4b, and the mechanical properties are summarized in Table 1. Both the pristine and MTES modified aerogels exhibited typical three-regime curves under compression in the longitudinal direction which are a characteristic of porous structures [28]. 1) initial elastic deformation at low strain before the yield point, corresponding to the elastic bending of cell walls; 2) a plastic yielding plateau where the strain increased while the stress almost remains unchanged, attributed to the progressive buckling of the channel walls; 3) a final densification stage at high strain where the stress increased rapidly with increasing strain. The bent pore walls start to touch each other at this stage which leads to stiffening behaviour [29]. For the same type of sample, a higher compression modulus and maximum stress values were observed in the longitudinal direction in comparison to the transverse direction. This is mainly due to the anisotropic aligned channel structure inside the aerogels, in which the tubular channel walls provide the aerogel with robust support and prevent vertical deformation under external forces, leading to increased modulus and maximum stress. In contrast, no apparent yield point was presented in the unmodified aerogel in the transverse direction, and the maximum stress at 80% strain is also much lower than the longitudinal direction. This is because the vertically aligned channel walls cannot bear high load from a direction perpendicular to its orientation. This agrees with other anisotropic aerogels in previous reports [26, 30]. Interestingly, the MTES modified aerogels exhibited a yield point at about 30% strain, a much longer elastic strain range and higher yield stress in comparison with the unmodified aerogels. This indicates that the liquid phase silane modification process was contributing to a better mechanical performance.

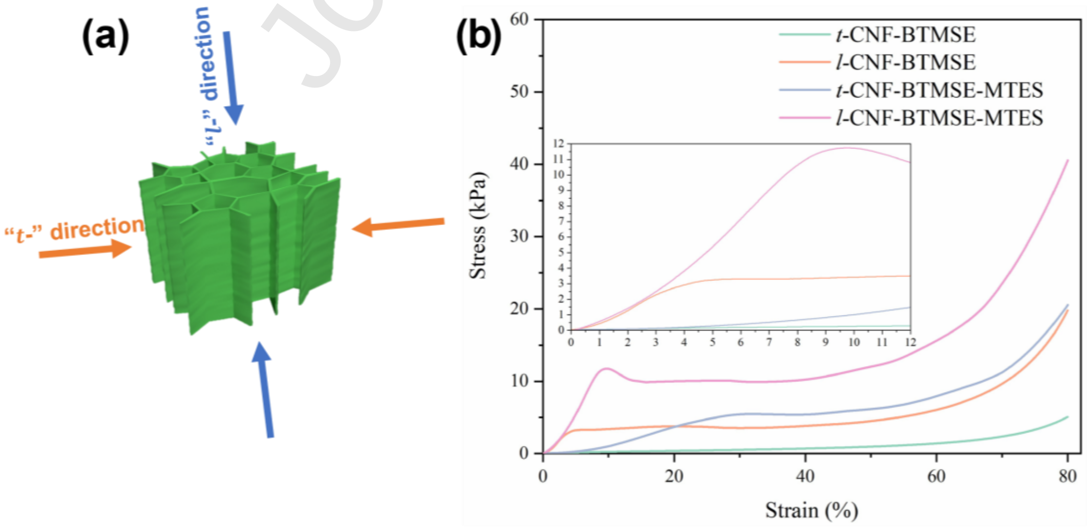

Fig. 4. (a) Schematic illustration of the anisotropic aerogel compressed in "*l*-" and "*t*-" directions, where "*l*-" and "*t*-" represent longitudinal direction (along the freezing direction), and transverse direction (perpendicular to freezing direction); (b) Stress-strain curves for the aerogels with and without MTES modification in two directions.

Table 1. Mechanical properties of CNF-BTMSE and CNF-BTMSE-MTES anisotropic aerogels

Samples	Compression modulus (kPa)	Maximum stress at 80% strain	Recovery rate at 80% strain
t-CNF-BTMSE	1.8 ± 0.2	5.1 ±0.6	77.3 ± 3.0
l-CNF-BTMSE	61.0 ± 6.2	19.8 ±1.1	58.6 ± 4.5
t-CNF-BTMSE-MTES	3.8 ± 0.3	20.5 ±1.3	85.8 ± 2.5
l-CNF-BTMSE-MTES	78.5 ± 8.3	40.5 ±1.9	50.2 ± 6.1

Although the compression modulus and strength of MTES modified aerogels are lower in the transverse direction, they exhibited a better resilience compared to the longitudinal direction. The aerogels can recover over 85% of their original height at a high strain rate of 80% in the transverse direction, while the shape recovery rate is only 52% in longitudinal direction. To further study its fatigue resistance, cyclic compression tests were performed in the transverse direction on the MTES modified aerogel within the strain range from 0-70% (Fig. 5a, and Video 1), and the resulting stress-strain curves are shown in Fig. 5b. The results showed that the aerogel retained about 65% of its compressive strength and recovered over 82% of its original height even after 100 cycles (Fig. 5c). A significant reduction in the compressive strength and shape recovery rate was observed in the second loading cycle. This is attributed to the plastic deformation in the channel walls from the first compression process. The overlapping of curves from approximately the thirtieth load cycle indicates that no new irreversible deformation occurred after a certain number of compressions, showing the good fatigue resistance and resilience performance of the aerogel. We believe that the excellent flexibility of the aerogel is mainly due to its anisotropic structure and hydrophobicity. Previous studies have highlighted achieving high compressibility and elasticity requires preventing the formation of strong hydrogen bonds between adjacent CNFs during compression, which would otherwise lead to permanent deformation and collapse of the material's structure [10, 28]. By applying a simple directional freezing process, honeycomb-like microstructure is achieved in the cross-section of cellulose aerogel. As shown in Fig. 5a, during compression, stress is uniformly distributed across the interconnected channel walls and the strain energy is stored in the deformed pores. Consequently, when the compressed aerogel is released, it quickly springs back to its original shape. Additionally, the MTES modification forms a polysiloxane coating on the cellulose surface which helps to weaken the hydrogen bonding interaction between CNFs [31], and the repulsive interaction between alkyl groups is also believed to provide extra repulsive forces at the microlevel [30, 32].

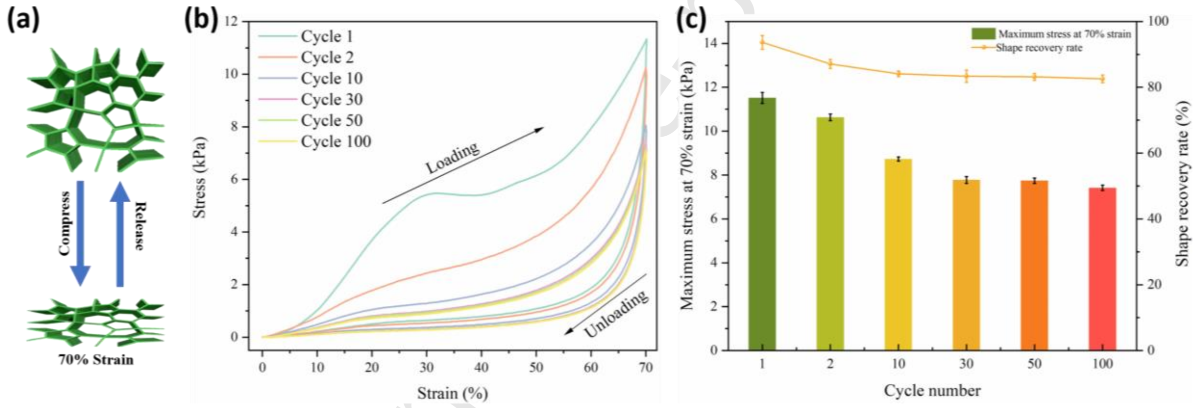

Fig. 5. (a) Schematic illustration of the shape changes of the anisotropic aerogel in the *t*-direction; (b) Cyclic compressive stress-strain curves; (c) Change of maximum stress at 70% strain and the corresponding shape recovery rates at each number of cycles.

3.3 Wettability of the MTES modified aerogel

The water contact angel (WCA) of the aerogel surface was measured to characterize its wettability. As shown in Fig. 6a, the aerogel without MTES modification is amphipathic, both water (dyed with methylene-blue) and corn oil droplets (dyed with Sudan-III) were instantly absorbed upon contact with the surface of the aerogel. No WCA was recorded due to the rapid adsorption process. In contrast, the MTES modified aerogels exhibited good hydrophobicity, absorbing only oil droplets, while water droplets formed a spherical shape on the surface. In addition, as shown in Fig. 6b a mirror reflection, caused by the trapped air between the aerogel surface and the surrounding water was observed when pushing the MTES modified aerogel underwater, further demonstrating the aerogel's outstanding hydrophobicity. The surface hydrophobicity of MTES modified aerogel is attributed to the synergistic effects of high surface roughness and low surface energy of the methyl-containing polysiloxane particles. Fig. 6c shows that as the concentration of MTES increased in the cellulose suspension, a higher WCA was measured on the aerogel surface. This is due to the formation of more polysiloxane particles on the surface of the freeze-dried aerogel. However, the aerogel's hydrophobicity stabilized at a WCA of about 142º at with 20 mmol/g of MTES added. Further addition of MTES did not lead to a higher WCA. This might be attributed to the combined effects of two factors that influence the surface wettability. At low MTES concentrations, the condensation of polysiloxane particles on the aerogel surface both introduce a lower surface energy and a higher surface roughness. However, when the MTES concentration exceeds a certain point, a thick polysiloxane particle layer may reduce the surface roughness which leads to a negative effect on the total surface hydrophobicity [33].

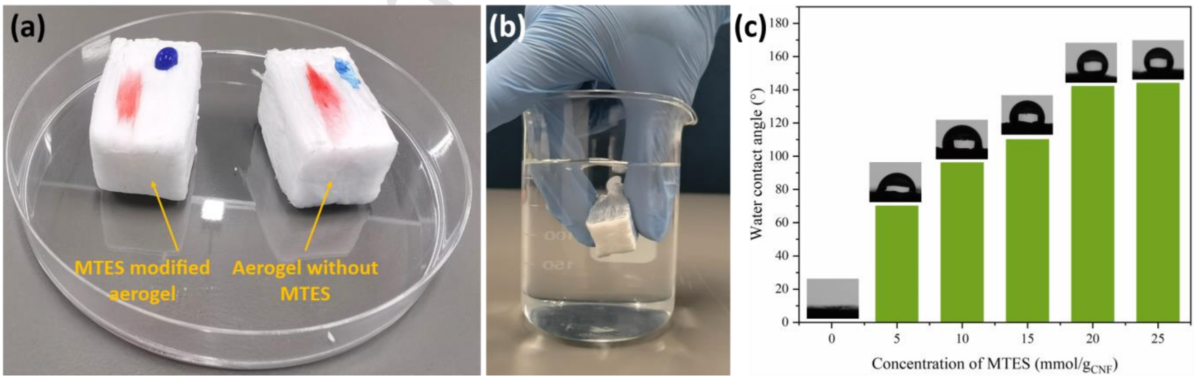

Fig. 6. (a) Comparison of the surface wettability of the MTES modified aerogel and the unmodified aerogel; (b) Mirror-reflection on the surface of the MTES modified aerogel; (c) The change of WCA of MTES modified aerogel as a function of the MTES concentration.

3.4 Oil adsorption capacity and reusability of the aerogel

Owing to its high hydrophobicity and oil adsorption selectivity, the 20 mmol/g MTES modified aerogel was selected for the oil adsorption testing. As shown in Fig. 7a, the aerogel quickly and completely absorbed the light corn oil (Sudan III-stained) and stayed afloat on the water surface when placed into the oil/water mixture. Furthermore, Fig. 7b demonstrates that the dichloromethane droplet was also absorbed by the aerogel when pushing it underwater. In addition to those two pollutants, various oils and organic solvents were tested to demonstrate the aerogel's outstanding adsorption capacities. As shown in Fig. 7c, depending on the pollutant densities, the adsorption capacities ranged from 80 – 105 g/g. During the adsorption process, the oil gradually enters and occupies the pore volumes of the aerogel, therefore, with similar adsorption volume, higher adsorption capacities were observed for the oils and organic solvents with higher densities (Fig. 7d). Compared with other reported oil sorbents, our anisotropic aerogel exhibited similar adsorption capacities to those of CNF-based ones, higher than wood and corn stalk sponges and the synthetic polymer foams, but slightly lower than BC aerogels (Table 2). However, the bacterial cellulose (BC) and CNF-based aerogels listed in the table all require a separate modification process after the aerogel is freeze-dried which is complicated and time-consuming. The aerogel in our work is simpler to fabricate and offers better reproducibility.

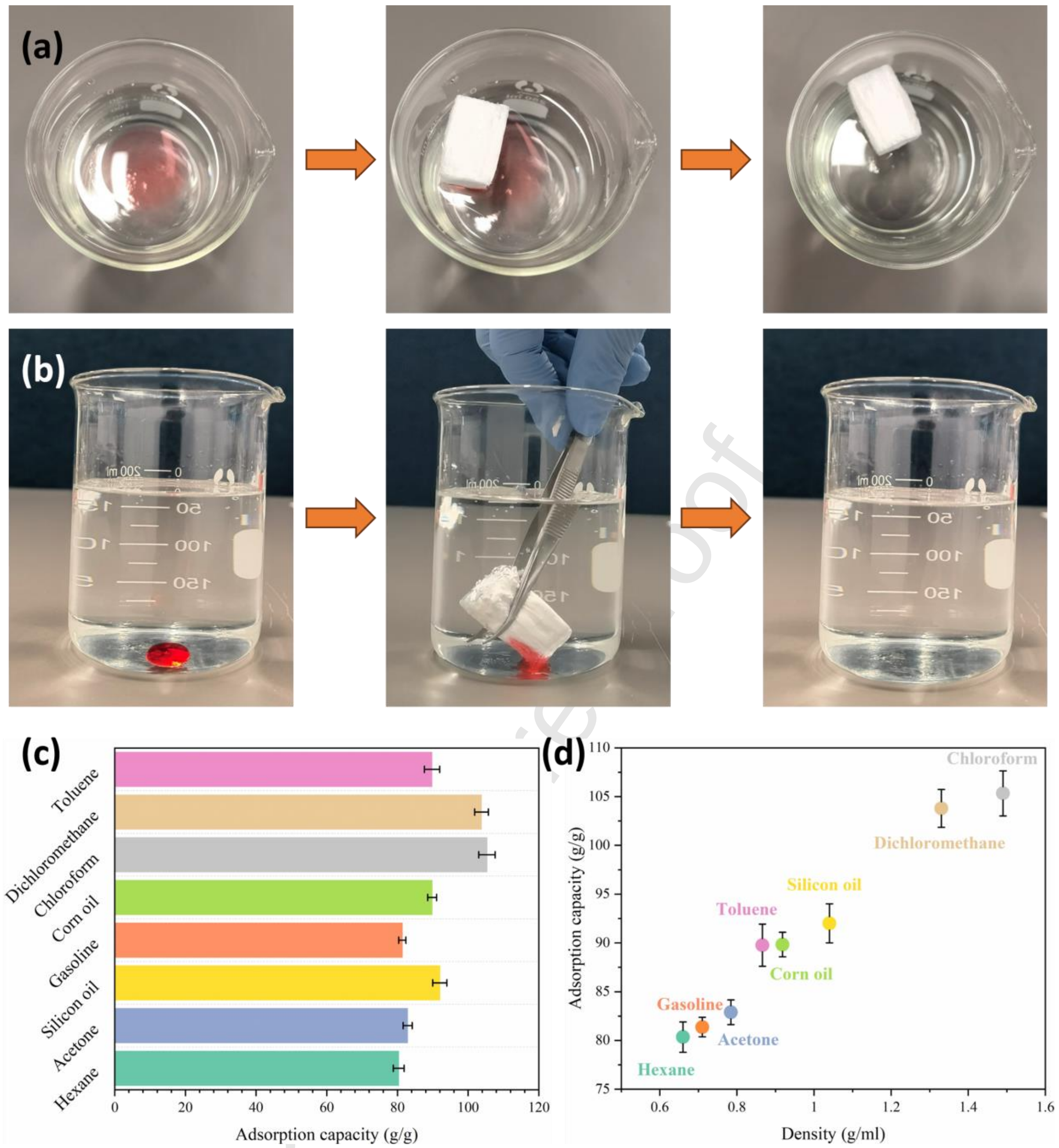

Fig. 7. (a) Selective removal of corn oil from the water surface by MTES-modified anisotropic aerogel; (b) Selectively absorbing dichloromethane; (c) Adsorption capacity of MTES-modified anisotropic aerogel for different oils and organic solvents; (d) Adsorption capacity of MTES-modified anisotropic aerogel as a function of pollutant densities.

Table 2. Comparison of the adsorption capacity of MTES-modified anisotropic aerogel with other 3-dimesional porous oil sorbents

Type	Absorbent	Modification method	Adsorption capacity (g/g)	Ref.
Synthetic polymers	Activated carbon enhanced thermoplastic polyurethane composite aerogel	TIPS	Up to 39.6	[34]
	Silylated Al_2O_3-polyimide foam	SIS	90	[35]
	Melamine formaldehyde composite foam	CVD	12-25	[36]
	poly (vinylidene fluoride) aerogel	Vapor induced phase inversion	3-7	[37]
Inorganic sorbents	PDMS/SiO_2 modified rock wool sponges	High temperature reaction	8-13	[38]
	rGO-SiO_2 composite aerogels	Co-gelation of TEOS and GO	7-10	[39]
Cellulose-based sorbent	Cellulose aerogel made from rice straw	CVD	Up to 170	[1]
	PVA-CNF aerogels	CVD	Up to 136	[40]
	Nanocellulose-based aerogel	CVD	78.8-162.4	[41]
	Magnetic hydrophobic cellulose aerogels	CVD	Up to 181	[42]

Abbreviations: **TIPS**, Thermally induced phase separation; **SIS**, Sequential infiltration synthesis; **CVD**, Chemical vapor deposition; **rGO**, reduced-graphene oxide; **TEOS**, Tetraethyl orthosilicate; **PVA**, Polyvinyl alcohol; **CNF**, cellulose nanofiber; **SI-ATRP**, surface-initiated atom transfer radical polymerization.

The reusability of the oil sorbent and recoverability of the absorbed oils are crucial for practical oily wastewater remediation. Herein, a mechanical squeeze test was employed to evaluate the MTES-modified anisotropic aerogel. The saturated aerogel was squeezed along the transverse direction using two parallel glass slides to eject the oil and then submerged in oil for the next adsorption cycle. The adsorption capacity was recorded after each cycle. Interestingly, as shown in Fig. 8a, while the aerogel did not fully spring back to its original height after squeezing, it nearly recovered to its original shape when submerged for the next adsorption. Additionally, as shown in Fig. 8b, ~85% of the adsorption capacity was retained compared to the initial value, even after 40 cycles. This result is superior to many of the previous reports [1, 43-45]. The excellent reusability is attributed to the aerogel's anisotropic structure, which provides the aerogel with good flexibility and elasticity. Therefore, the MTES modified aerogels are ideal oil sorbents for oil-spill cleanup and oily wastewater remediation.

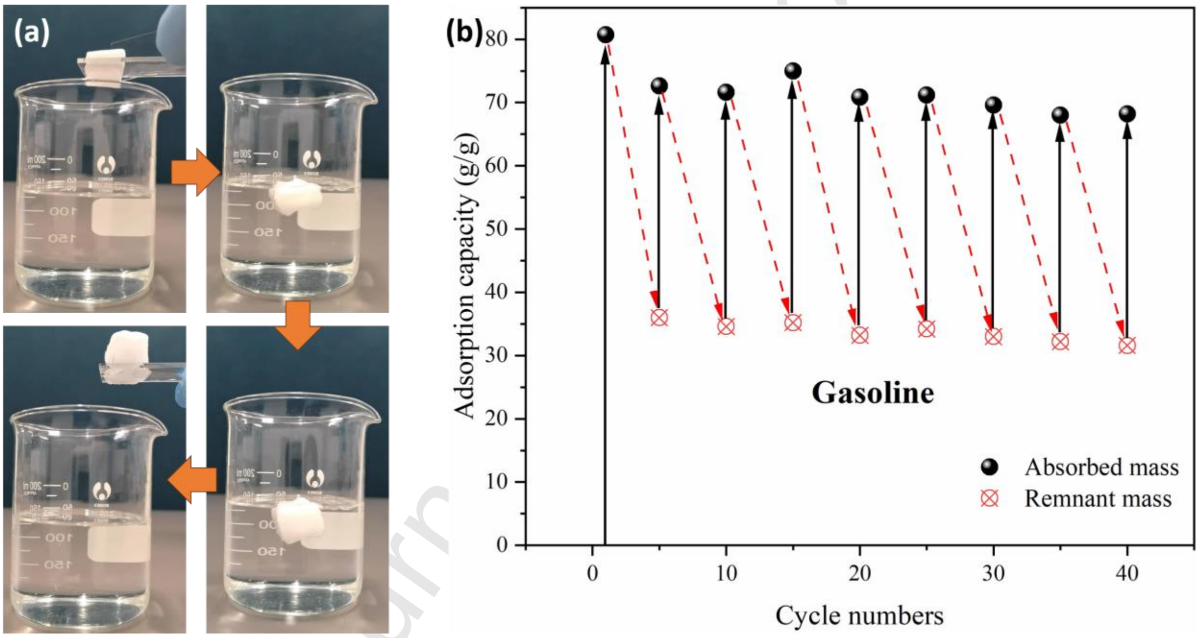

Fig. 8. (a) Shape recovery of the MTES-modified anisotropic aerogel after absorbing gasoline; (b) The adsorption capacity of MTES-modified anisotropic aerogel for gasoline after each compression-adsorption cycle.

3.5 Oil adsorption kinetics of the MTES modified aerogel

To study the adsorption kinetics of MTES modified aerogels, corn oil and gasoline were used as the test oils for obtaining the experimental adsorption data. Two adsorption models, pseudo-first order

(Eq. 8) and pseudo-second order (Eq. 9) models were employed to fit the experimental adsorption data [46].

$$\ln(q_e - q_t) = lnq_e - k_1 t \tag{8}$$

$$q_\mathrm{t} = \frac{k_2 q_e^2 \mathrm{t}}{1+k_2 q_\mathrm{e} t} \tag{9}$$

where q_e (g/g) and q_t (g/g) are the equilibrium adsorption capacity and the adsorption capacity at time t, respectively. t (s) is time. k_1 and k_2 are the sorption rate constants.

The model fit was evaluated by calculating the root-mean-square-deviation (RMSD), defined by Eq. 10 as follows:

$$\mathrm{RMSD} = \sqrt{\frac{\Sigma(q_{t(\exp)} - q_{t(fit)})}{\mathrm{N}}} \tag{10}$$

where N is the number of experimental points and its value is 13, $q_{t(\mathrm{exp})}$ (g/g) is the experimental adsorption capacity data at time t, and $q_{t(\mathrm{fit})}$ (g/g) is the adsorption capacity value taken at time t from the fitted curve.

The adsorption kinetics fitted curves are shown in Fig. 9, and the parameters of the two adsorption kinetic models are provided in Table 3. The experimental data demonstrates that the adsorption was rapid during the initial stages and then leveled off. This behavior is attributed to the porous structure of the aerogel. A large amount of pores are available for adsorption at the initial stages, however, as adsorption progresses, the remaining pores become more difficult for the oil to occupy because of the repulsive force between the oil molecules [47]. The viscosity of the oil also influences the adsorption rate; higher viscosity results in slower intermolecular movement and reduced fluidity [48]. The aerogel reached adsorption equilibrium in approximately 22 s for gasoline, whereas it took about 35 s to reach equilibrium for the adsorption of higher viscosity corn oil. Comparing the two fitted curves, the pseudo-first order model shows a higher R^2 value and lower RMSD that indicates it is more suitable for describing the oil adsorption behavior of this MTES modified anisotropic aerogel.

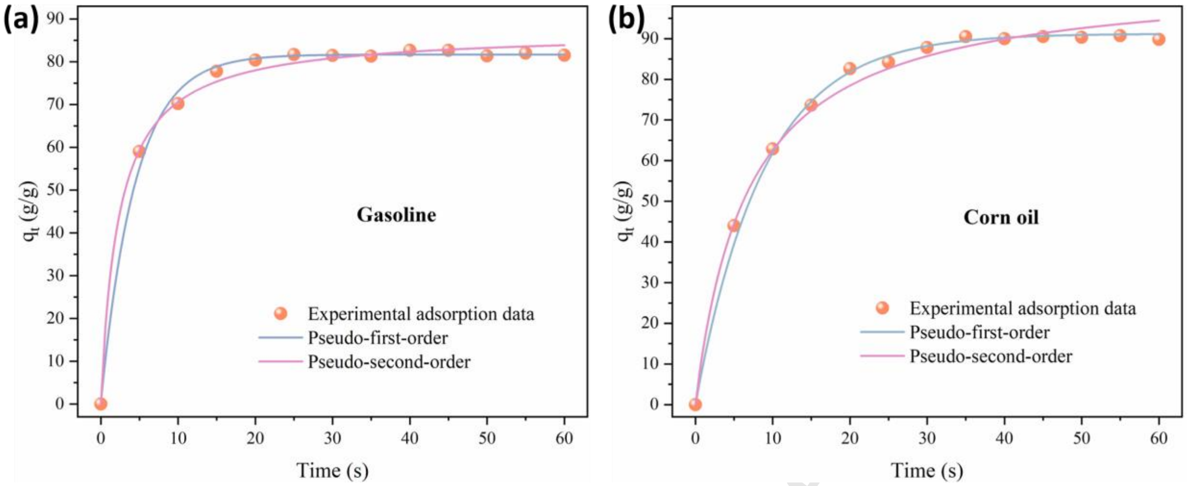

Fig. 9. Sorption kinetics of (a) gasoline, and (b) corn oil absorbed by MTES-modified anisotropic aerogel.

Table 3. Parameters of pseudo-first order and pseudo-second order models in fitting the experimental oil adsorption data

Oils	Pseudo-first order				Pseudo-second order			
	k_1	q_e	R^2	RMSD	k_2	q_e	R^2	RMSD
Gasoline	0.088	81.36	0.995	2.95	0.0048	85.24	0.986	4.75
Corn oil	0.12	89.81	0.995	3.86	0.0086	93.24	0.979	5.01

3.6 Water-in-oil (W/O) emulsion separation

In addition to adsorption, the modified aerogels were further tested for separating water-in-oil emulsions through a filtration method. As another category of oil/water mixture, emulsions are not suitable for separation by adsorption. Finding an inexpensive strategy to separate surfactant-stabilized emulsions remains a significant challenge. Three types of water-in-oil emulsions, including water-in-corn oil, water-in-toluene, and water-in-dichloromethane were used for the filtration experiments. All emulsions were stabilized with Span 80 as stabilizer at a concentration of 0.1 wt%. The emulsions were effectively stabilized without any demulsification visible after one month at room temperature. As shown in Fig. 10a, the filtration process was simply achieved by pouring the emulsions over the aerogel in a funnel; the separation process was driven solely by gravity. The milky emulsion was successfully separated by the aerogel, and the filtrate was clean and transparent (Fig. 10b). The high hydrophobicity and superoleophilicity of the aerogel are believed to be the key factors contributing to this exceptional separation efficiency. When the emulsion contacted the aerogel, the oil phase was instantly absorbed by the aerogel, resulting in the formation of a thin oil layer on the aerogel surface; while the water droplets were blocked and filtered out because of the high hydrophobicity of the aerogel. As the emulsion flowed continuously, more water droplets were blocked, coalescence and agglomeration appeared, resulting in the demulsification of the W/O emulsion and eventually the separation of oil and water phases. Optical microscope images were taken from the feeds and filtrates to show the separation efficiency. Water droplets ranging in sizes between 2-8 μm were observed in the feed emulsions, whereas a clear and continuous oil phase without any water droplets was observed in the filtrate, indicating the superhigh separation efficiency (Fig. 10b). Moreover, a high flux of 782 L m^{-2} h^{-1} was observed when pouring the emulsion into the funnel at a 10 cm height. The separation efficiencies of MTES-modified anisotropic cellulose aerogel towards the three emulsions ranged from 98.7-99.2%.

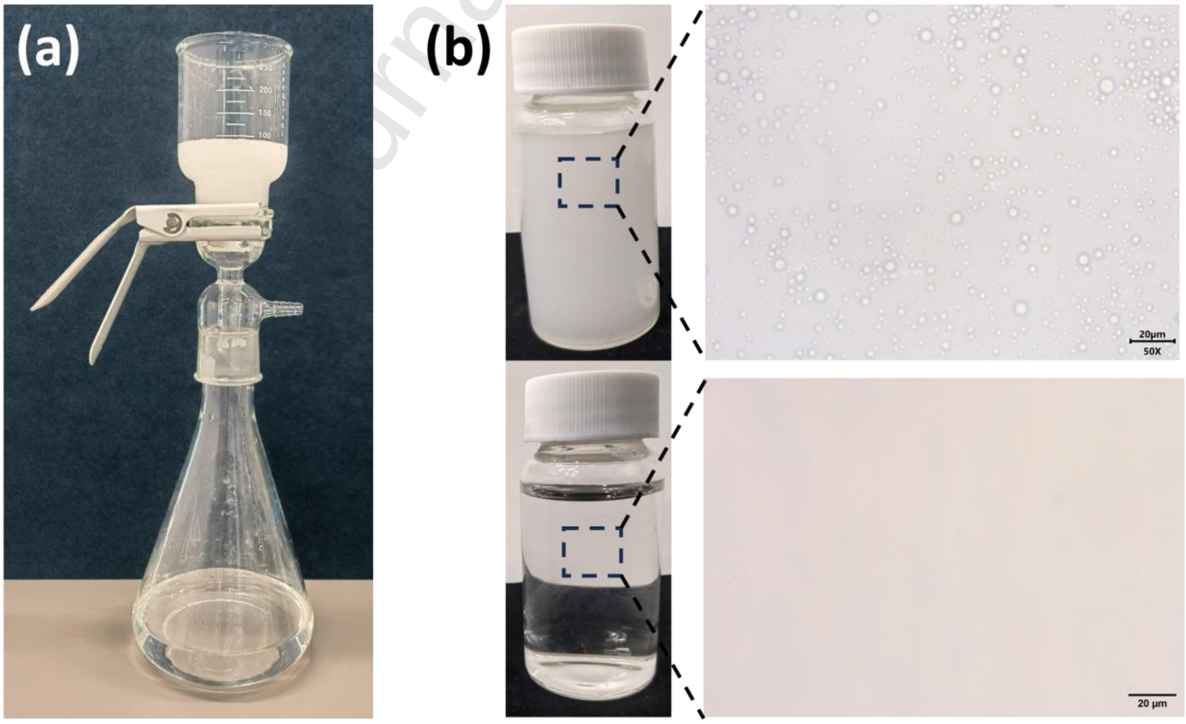

Fig. 10. (a) The gravity driven water-in-oil separation setup; (b) Photographic and optical microscope images showing the water-in-oil emulsion (above), and the filtrate oil (below).

4. Conclusion

In summary, hydrophobic superelastic, anisotropic CNF-based aerogels were successfully fabricated through a facile one-pot synthesis strategy followed by a directional freeze-drying. This method allowed for simultaneous crosslinking and hydrophobic modification of cellulose nanofibers (CNFs) in an aqueous state before drying, significantly simplifying the preparation process for hydrophobic cellulose-based aerogels. Moreover, this approach achieved a more uniform hydrophobic modification throughout the aerogel compared to conventional gaseous-phase chemical vapor deposition. The directional freeze-drying process resulted in an anisotropic structure with aligned channels in a honeycomb like morphology in cross-section. This unique structure provides the aerogel with superelasticity, allowing it to recover 85% of the original height after 100 compression-release cycles. Due to these advantages, the MTES-modified anisotropic aerogel achieved a high oil adsorption capacity of 80 – 105 g/g for various oils and organic solvents, as well as excellent reusability. Furthermore, when used as a filter, a high flux of 782 L m^{-2} h^{-1} and high separation efficiency of up to 99.2% was observed for the separation of water-in-oil emulsions. Therefore, such aerogels are highly promising candidates to be used for oily wastewater remediation.

References

1. Dilamian, M. and B. Noroozi, *Rice straw agri-waste for water pollutant adsorption: Relevant mesoporous super hydrophobic cellulose aerogel.* Carbohydrate Polymers, 2021. **251**: p. 117016.
2. Dong, T., G. Xu, and F. Wang, *Adsorption and adhesiveness of kapok fiber to different oils.* Journal of Hazardous Materials, 2015. **296**: p. 101-111.
3. Behnood, R., et al., *Oil spill sorption using raw and acetylated sugarcane bagasse.* Journal of Central South University, 2016. **23**: p. 1618-1625.
4. Ali, N., et al., *Characteristics and oil sorption effectiveness of kapok fibre, sugarcane bagasse and rice husks: oil removal suitability matrix.* Environmental technology, 2012. **33**(4): p. 481-486.

5. Oribayo, O., et al., *Synthesis of lignin-based polyurethane/graphene oxide foam and its application as an absorbent for oil spill clean-ups and recovery.* Chemical Engineering Journal, 2017. **323**: p. 191-202.
6. Renuka, S., R. Rengasamy, and D. Das, *Studies on needle-punched natural and polypropylene fiber nonwovens as oil sorbents.* Journal of Industrial Textiles, 2016. **46**(4): p. 1121-1143.
7. Prasad, C., et al., *Review on recent advances in cellulose nanofibril based hybrid aerogels: Synthesis, properties and their applications.* International Journal of Biological Macromolecules, 2024. **261**: p. 129460.
8. Gao, J., et al., *Advanced superhydrophobic and multifunctional nanocellulose aerogels for oil/water separation: A review.* Carbohydrate Polymers, 2022: p. 120242.
9. Meng, Y., et al., *Ultralight carbon aerogel from nanocellulose as a highly selective oil absorption material.* Cellulose, 2015. **22**(1): p. 435-447.
10. Mi, H.-Y., et al., *Highly compressible ultra-light anisotropic cellulose/graphene aerogel fabricated by bidirectional freeze drying for selective oil absorption.* Carbon, 2018. **132**: p. 199-209.
11. Zhou, L. and Z. Xu, *Ultralight, highly compressible, hydrophobic and anisotropic lamellar carbon aerogels from graphene/polyvinyl alcohol/cellulose nanofiber aerogel as oil removing absorbents.* Journal of hazardous materials, 2020. **388**: p. 121804.
12. Pham, V.H. and J.H. Dickerson, *Superhydrophobic silanized melamine sponges as high efficiency oil absorbent materials.* ACS applied materials & interfaces, 2014. **6**(16): p. 14181-14188.
13. Chen, F., et al., *Wood-inspired elastic and conductive cellulose aerogel with anisotropic tubular and multilayered structure for wearable pressure sensors and supercapacitors.* International Journal of Biological Macromolecules, 2023. **250**: p. 126197.
14. Si, Y., et al., *Ultralight nanofibre-assembled cellular aerogels with superelasticity and multifunctionality.* Nature Communications, 2014. **5**(1): p. 5802.
15. Gao, J., et al., *Advanced superhydrophobic and multifunctional nanocellulose aerogels for oil/water separation: A review.* Carbohydrate Polymers, 2023. **300**: p. 120242.
16. Zhai, Y. and X. Yuan, *Superhydrophobic, Magnetic Aerogels Based on Nanocellulose Fibers Derived from Harakeke for Oily Wastewater Remediation.* Polymers, 2023. **15**(19): p. 3941.
17. Zhai, Y., et al., *Superhydrophobic cellulose-based aerogel derived from Phormium tenax (harakeke) for efficient oil sorption.* Industrial Crops and Products, 2023. **202**: p. 116981.
18. Zhang, X., et al., *Ultralight, hydrophobic, anisotropic bamboo-derived cellulose nanofibrils aerogels with excellent shape recovery via freeze-casting.* Carbohydrate polymers, 2019. **208**: p. 232-240.
19. Li, L., et al., *Compressible and conductive carbon aerogels from waste paper with exceptional performance for oil/water separation.* Journal of Materials Chemistry A, 2017. **5**(28): p. 14858-14864.
20. Fan, F., et al., *Extraction and characterization of cellulose nanowhiskers from TEMPO oxidized sisal fibers.* Cellulose, 2022. **29**(1): p. 213-222.
21. Cao, X., et al., *Cellulose nanowhiskers extracted from TEMPO-oxidized jute fibers.* Carbohydrate Polymers, 2012. **90**(2): p. 1075-1080.
22. Wu, Z., et al., *One-pot fabrication of hydrophilic-oleophobic cellulose nanofiber-silane composite aerogels for selectively absorbing water from oil–water mixtures.* Cellulose, 2021. **28**(3): p. 1443-1453.
23. Hayami, R., et al., *Soluble ethane-bridged silsesquioxane polymer by hydrolysis–condensation of bis(trimethoxysilyl)ethane: characterization and mixing in organic polymers.* Journal of Polymer Research, 2020. **27**(10): p. 316.
24. Fan, B., et al., *Highly compressible and hydrophobic nanofibrillated cellulose aerogels for cyclic oil/water separation.* International Journal of Biological Macromolecules, 2023. **242**: p. 125066.

25. Yan, Z., et al., *Recyclable Bacterial Cellulose Aerogel for Oil and Water Separation.* Journal of Polymers and the Environment, 2022. **30**(7): p. 2774-2784.
26. Fan, B., et al., *High capillary effect and solar dual-drive nanofibrillated cellulose aerogels for efficient crude oil spill cleanup.* Chemical Engineering Journal, 2024. **480**: p. 148149.
27. Li, J., et al., *Ultra-light, compressible and fire-resistant graphene aerogel as a highly efficient and recyclable absorbent for organic liquids.* Journal of Materials Chemistry A, 2014. **2**(9): p. 2934-2941.
28. Qin, H., et al., *Multifunctional Superelastic Cellulose Nanofibrils Aerogel by Dual Ice‐Templating Assembly.* Advanced Functional Materials, 2021: p. 2106269.
29. Sehaqui, H., et al., *Mechanical performance tailoring of tough ultra-high porosity foams prepared from cellulose I nanofiber suspensions.* Soft Matter, 2010. **6**(8): p. 1824-1832.
30. Zhang, X., et al., *Highly Compressible and Hydrophobic Anisotropic Aerogels for Selective Oil/Organic Solvent Absorption.* ACS Sustainable Chemistry & Engineering, 2019. **7**(1): p. 332-340.
31. Guan, H., Z. Cheng, and X. Wang, *Highly Compressible Wood Sponges with a Spring-like Lamellar Structure as Effective and Reusable Oil Absorbents.* ACS Nano, 2018. **12**(10): p. 10365-10373.
32. Zhang, Z., et al., *Ultralightweight and flexible silylated nanocellulose sponges for the selective removal of oil from water.* Chemistry of Materials, 2014. **26**(8): p. 2659-2668.
33. Niu, H., et al., *Solar-assisted, fast, and in situ recovery of crude oil spill by a superhydrophobic and photothermal sponge.* ACS Applied Materials & Interfaces, 2021. **13**(18): p. 21175-21185.
34. Wang, Q., et al., *A thermoplastic polyurethane-based composite aerogel with low shrinkage and high specific surface area enhanced by activated carbon for highly efficient oil/water separation.* Journal of Environmental Chemical Engineering, 2023. **11**(5): p. 111077.
35. Barry, E., et al., *Advanced oil sorbents using sequential infiltration synthesis.* Journal of Materials Chemistry A, 2017. **5**(6): p. 2929-2935.
36. Jin, H., et al., *Multifunctional Melamine Formaldehyde Composite Foam for High-Temperature Insulation, Flame Retardancy, and Oil–Water Separation.* Industrial & Engineering Chemistry Research, 2022. **61**(19): p. 6458-6467.
37. Chen, X., et al., *Additive-free poly (vinylidene fluoride) aerogel for oil/water separation and rapid oil absorption.* Chemical Engineering Journal, 2017. **308**: p. 18-26.
38. Hao, W., et al., *Developing superhydrophobic rock wool for high-viscosity oil/water separation.* Chemical Engineering Journal, 2019. **368**: p. 837-846.
39. Thakkar, S.V., et al., *Performance of oil sorbents based on reduced graphene oxide–silica composite aerogels.* Journal of Environmental Chemical Engineering, 2020. **8**(1): p. 103632.
40. Xu, Z., et al., *Preparation of magnetic hydrophobic polyvinyl alcohol (PVA)–cellulose nanofiber (CNF) aerogels as effective oil absorbents.* Cellulose, 2018. **25**(2): p. 1217-1227.
41. Rafieian, F., et al., *Development of hydrophobic nanocellulose-based aerogel via chemical vapor deposition for oil separation for water treatment.* Cellulose, 2018. **25**(8): p. 4695-4710.
42. He, X., et al., *Preparation and adsorption properties of magnetic hydrophobic cellulose aerogels based on refined fibers.* Carbohydrate Polymers, 2021. **260**: p. 117790.
43. Gong, X., et al., *Highly porous, hydrophobic, and compressible cellulose nanocrystals/poly (vinyl alcohol) aerogels as recyclable absorbents for oil–water separation.* ACS Sustainable Chemistry & Engineering, 2019. **7**(13): p. 11118-11128.
44. Nguyen, T.T.V., et al., *Synthesis, Characteristics, Oil Adsorption, and Thermal Insulation Performance of Cellulosic Aerogel Derived from Water Hyacinth.* ACS omega, 2021. **6**(40): p. 26130-26139.
45. Yin, T., et al., *Cellulose-based aerogel from Eichhornia crassipes as an oil superabsorbent.* RSC advances, 2016. **6**(101): p. 98563-98570.

46. Yan, C., et al., *Superadsorbent aerogel based on sunflower stem pith cellulose and layered double hydroxides modified montmorillonite for methylene blue removal from water solution.* International Journal of Biological Macromolecules, 2024. **257**: p. 128749.
47. Lazzari, L.K., et al., *A study on adsorption isotherm and kinetics of petroleum by cellulose cryogels.* Cellulose, 2019. **26**(2): p. 1231-1246.
48. Liu, Q., et al., *Preparation of antifouling and highly hydrophobic cellulose nanofibers/alginate aerogels by bidirectional freeze-drying for water-oil separation in the ocean environment.* Journal of Hazardous Materials, 2023. **441**: p. 129965.

Declaration of interests

☒The authors declare that they have no known competing financial interests or personal relationships that could have appeared to influence the work reported in this paper.

☐The authors declare the following financial interests/personal relationships which may be considered as potential competing interests:

Highlights

- Anisotropic cellulose nanofiber-based aerogel with superelasticity was obtained by directional freeze-casting.
- Harakeke fiber is converted into cellulose-based aerogel by a simple and efficient fabrication process.
- The crosslinking of individual cellulose-nanofibers and the hydrophobization of pristine cellulose were achieved simultaneously in a facile one-pot strategy before the drying process.
- The aerogel shows high oil adsorption capacity and excellent water-in-oil emulsion separation efficiency.